Electron-nuclear dynamics of multiphoton H_2^+ dissociative ionization in intense laser fields

S. Chelkowski, C. Foisy, and A. D. Bandrauk
Laboratoire de Chimie Théorique, Faculté des Sciences, Université de Sherbrooke, Sherbrooke, Québec, Canada J1K 2R1
(Received 26 June 1997)

The time-dependent Schrödinger equation for the one-dimensional H_2^+ molecule (with both nuclear and electronic degrees of freedom included) was solved numerically to study dissociative ionization. A wave-function splitting technique was used with projections onto Volkov states, which allows one to circumvent the problem of lost information on electron flux due to absorbing boundary methods. This technique allows us to calculate the above-threshold ionization (ATI) photo electron kinetic-energy spectra in the presence of moving nuclei, as well as complete spectra of dissociating protons, beyond the Born-Oppenheimer approximation. The ATI spectra are considerably enhanced with respect to the H-atom spectra due to electron molecule interaction. The peaks seen in calculated Coulomb explosion spectra of protons agree well with recent theoretical and experimental work related to the phenomenon of charge-resonance-enhanced ionization in molecules. [S1050-2947(98)05302-5]

PACS number(s): 42.50.Hz

I. INTRODUCTION

The interaction of intense laser pulses (intensity $I > 10^{13}$ W/cm^2) with atoms and molecules leads to many new interesting multiphoton, nonperturbative phenomena such as high-order harmonic generation, above-threshold dissociation (ATD), and above-threshold ionization (ATI). This has been an area of active research in the past decade [1–5], and there has been extensive progress in the understanding of these processes in atoms. The situation for molecules is not as advanced because of the complexity arising from the additional nuclear degrees of freedom. Despite the fact that the electronic and nuclear characteristic time scales are very different (attosecond, 10^{-18} s, vs femtosecond, 10^{-15} fs), the intense laser field induces a complex correlation between both motions, which we attempt to study by solving numerically the time-dependent Schrödinger equation (TDSE) using the exact, one-dimensional (1D), three-body Hamiltonian for a H_2^+ molecular ion in an intense, linearly polarized laser field. We have reported earlier results of simulations based on the TDSE for H_2^+ with a single 3D electron and 1D protons for 212 and 600-nm wavelengths [6,7]. Similar calculations for 1D electrons and protons were also reported recently [8,9]. In all these studies absorbing boundaries were used to remove the electron flux from the finite electron grid (in Refs. [8, 9], a nuclear absorber was used as well). Therefore, so far, ATI kinetic spectra in the presence of moving nuclei have not been calculated. Similarly, removing the electron flux introduces loss of information about Coulomb exploding protons, with which the lost electron flux was linked (i.e., the $p+p+e^-$ channel), and consequently the high-energy part of the reported proton spectrum was incomplete. In the present paper we report the first, to our knowledge, complete calculations of Coulomb explosion spectra of protons and the ATI electron kinetic energy spectra from the dissociating H_2^+. The difficulty with the lost information of dynamics through absorbing boundaries is overcome with the help of a wave-function splitting technique [10,11] which allows us to propagate in time the absorbed part of the wave function in the asymptotic region using a much faster algorithm than that used in the zone close to nuclei [12–14]. We first describe this technique for frozen internuclear distance, in detail, in Sec. II of our paper. In Sec. III we present details of our exact, non-Born-Oppenheimer calculations, i.e., with both electron and nuclear motion, and show how the wave-function splitting technique is implemented for this case. In Sec. IV, we present the kinetic-energy spectra of the dissociating nuclear fragments, which show clear signatures of the charge-resonance-enhanced-ionization (CREI) phenomenon, and competition between ATD and Coulomb explosion. CREI was first discussed in Ref. [15] in relation to high-order harmonic generation, and was further studied using models with frozen nuclear motion [16–19] to interpret experimental Coulomb explosion results. Thus it remained to be investigated whether the effect of enhanced ionization would be washed out by the nuclear dynamics. Our previous non-Born-Oppenheimer calculations [6,7] did not show very clear CREI peaks in the proton spectra due to the above-mentioned electron flux losses through the absorbing boundaries. In contrast, the wavefunction splitting technique yields sharp Coulomb explosion peaks due to CREI, and also a weaker peak originating from the center of the initial wave packet. Section V contains the ATI electron spectra from H_2^+, showing considerable enhancement of peaks with respect to the H atom, both in the low- and high-energy parts: a very broad high-energy tail in the energy spectra of electrons is seen, extending up to $16U_p$, where $U_p = e^2E_M^2/4m\omega^2$ is the electron ponderomotive energy. Typically, the bulk of (about 99%) ionized electrons have strong ATI peaks in the energy range less than $3U_p$ (this limit corresponds to the maximum drift velocity for electrons born in the continuum with zero kinetic energy [20]). Recently, it was pointed out that, contrary to the harmonic generation spectra, the ATI electron spectra do not have a sharp cutoff but extend much further than $3U_p$ due to the rescattering of an electron returning to the nucleus [20–23]. So far these effects were much discussed for ATI from atoms. Recent measurements of extremely hot (multi-keV electrons ejected from a xenon cluster [24] suggest that these rescattering effects may be much stronger in molecules and clusters than in

simple atoms, since the electrons ionizing toward neighboring dissociating nuclei can scatter on them and absorb additional photons. Obviously, such a possibility does not exist in atoms or atomic ions. Therefore, hot electrons are less likely in atoms, since they can originate only from the returning electrons scattered on one nucleus, while in the dissociating molecule an ionizing electron can encounter another scatterer directly on its path on which additional photons can be absorbed. The investigation of this issue is the main focus of Sec. V. In the present paper, we use a 1D model for both electronic and nuclear degrees of freedom.

It appears that the 1D dynamics describes reasonably well the movement of the atomic electrons [2] in the linearly polarized, intense laser fields ($I \geqslant 10^{14}$ W/cm^2) and reproduces correctly such phenomena as high harmonic generation or ATI. Since the molecules in intense fields are aligned, due to the torque from laser induced polarizabilities [25], one may expect that 1D molecular dynamics can also reproduce most salient features of the dynamics in intense laser fields [($I \geqslant 10^{14}$ W/cm^2, i.e., above the ionization threshold)] in particular in the long-wavelength regime, when the the molecule dissociates via the bond softening mechanism [4,26,27] due to laser-induced avoided crossings [7]. Such a 1D molecular-dynamics calculation was presented recently [8,9]. It appears that the potential surfaces resulting from 1D electron motion are quite close to exact 3D surfaces, thus providing a model for nuclear motions with correct molecular harmonic and anharmonic constants as well as correct dissociation energy [8]. For instance the dissociation energy in our model is 2.879 eV, whereas its experimental value is 2.651 eV, and the separation of the two lowest vibrational levels is in the 1D model is 0.253 eV, whereas in the exact 3D model its value is 0.274.

II. DESCRIPTION OF THE WAVE-FUNCTION SPLITTING ALGORITHM FOR SOLVING THE TIME-DEPENDENT SCHRÖDINGER EQUATION

One of the theoretical approaches to calculate the ATI spectra relies on exact numerical solutions of the TDSE on recently available powerful supercomputers. So far this approach has been successfully applied to one-electron atoms and molecules (or two 1D electrons [28]). Typically, in such numerical simulations, the initial wave function of the electron is well localized in space, and later becomes spread over very large distances. At the end of a short intense 40-fs laser pulse, the front edge of the wave packet of the ionizing electron can be as far as 4000 a.u. from the nucleus (for $I=2\times10^{14}$ and $\lambda=600$ nm) and continues to expand for longer times. Thus in order to avoid reflections from the boundaries, prohibitively large boxes (grids with 32 000 points or more), in which the electron wave packet is fully contained, must be used. The most common solution to this difficulty is to use much smaller boxes with absorbing boundary conditions. This approach allows us to calculate the ionization rates and harmonic generation spectra, but does not allow us to calculate the photoelectron (or ATI) spectra (nor the accompanying Coulomb explosion in the molecular case) since the external part of the wave function is absorbed and lost. Also, in our recent 3D numerical studies of competition between ionization and dissociation [6,7] the use of absorber for the electron flux led to a considerable loss of information about the nuclear movement, i.e., we were unable to reproduce completely the spectra of dissociating fragments from the Coulomb explosion channel, since these fragments were linked with the absorbed electron flux. In this paper we develop a technique which allows us to reconstruct the total absorbed electron wave packet in momentum space and propagate it in time, analytically, to any time after the pulse turn-off. Thus with the help of this technique one can calculate efficiently the photoelectron spectra after the turn-off of the pulse. A similar technique has been earlier used [12], for calculating kinetic-energy spectra of photodissociation products (without ionization), with the laser-molecule coupling neglected in the asymptotic region. Recently [13], this technique was generalized for nondecaying (for large distances) dipole couplings (for dissociating molecules) and for the calculation of atomic ATI spectra from the time-dependent Schrödinger equation [14] at high frequencies. In the present work we extend this technique for solving the TDSE for molecules with moving nuclei by projecting onto asymptotic Volkov states. Since the wave-function splitting technique is quite complex in practice, we first, present this technique for the case of frozen nuclei, and explain in Sec. III how the technique was implemented for the case when the nuclei move. Therefore, in this section, the R variable is a fixed parameter, which we do not include in the wave function. Let us consider a time-dependent, 1D Schrödinger equation written (in a.u.) in the following forms:

$$i\,\frac{\partial\psi(z,t)}{\partial t}=\left(-\frac{1}{2}\,\frac{\partial^2}{\partial z^2}+V_C(z,R)+zE(t)\right)\psi(z,t), \quad (1)$$

where

$$V_C(z,R)=-\frac{1}{\sqrt{1+(z-R/2)^2}}-\frac{1}{\sqrt{1+(z+R/2)^2}}, \quad (2)$$

and $E(t)$ is the laser electric field. This equation is usually discretized and solved numerically for $|z|<z_M$, where z_M is a grid size. We tested the splitting method [10] for the case of a 1D H atom in the laser field of intensity $I=2.2\times10^{14}$ W/cm^2, $\lambda=630$ nm and $t_p=20$ cycles (one cycle equals 2.17 fs). We compared our results with the exact large grid calculations from Ref. [23]. The photoelectron spectra from this reference show a plateau extending up to $8U_p=70$ eV with a slowly decaying tail up to 130 eV (70 photons absorbed), where $U_p=e^2E_M^2/(4m\omega^2)$ is the electron ponderomotive energy. Thus the fastest electron has a speed $v_M=2.3$ a.u. and in $t_p=43$ fs can be as far as 4050 a.u.. Typically, the integration step in space is $\delta z=0.25$ a.u., which means that grids with over 32 000 grid points must be used for a 43-fs pulse. For n times longer pulses, n time greater grids should be used. This constitutes a serious difficulty, even for 1D problems. Therefore, a fast algorithm for large z's is very desirable. In particular, since the Coulomb forces are negligible for large z's, larger integration steps in space δz, as well as much larger steps in time, can be used asymptotically.

Let us divide the total grid into three overlapping regions in space, in which different evolution algorithms will be

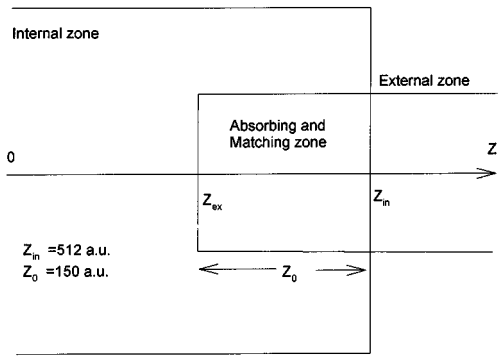

FIG. 1. Illustration of the two zones used in the wave-function splitting technique

used: the internal and two external (asymptotic, for positive and negative z's) parts defined by

$$\text{internal:} \quad |z|<z_{\text{in}}; \quad \text{external:} \quad z_{\text{ex}}<|z|<z_M, \tag{3}$$

where $z_{\text{in}}-z_{\text{er}}=z_0>0$ is the size of the overlap of both regions. Both regions are shown in Fig. 1 for positive z values (similar two boxes are used for negative z values). In the overlapping (or ''matching'') region an absorbing potential is introduced, which we have chosen in the following form:

$$V_{\text{abs}}(z)=iV_0\left(\frac{z-z_{\text{ex}}}{z_0}\right)^2 \quad \text{for } z_{\text{ex}}<|z|<z_{\text{in}}. \tag{4}$$

The electron wave function $\psi(z,t)$ is split into internal ψ_{int} and external ψ_{ext} parts, by applying this absorbing potential in the overlapping region of width z_0, at times $t_k=k\delta t$ where δt is much larger than the integration time dt ($dt=0.03$ a.u., $\delta t=150dt=0.05$ cycle, i.e., in our simulations for $\lambda=600$ nm, δt is much less than the laser cycle) with the help of the following formulas:

$$\psi(z,t)=\psi_{\text{in}}(z,t)+\psi_{\text{ex}}(z,t), \tag{5}$$

$$\psi_{\text{in}}(z,t)=f(z,\delta t)\psi(z,t), \tag{6}$$

$$\psi_{\text{ex}}(z,t)=[1-f(z,\delta t)]\psi(z,t), \tag{7}$$

where

$$f(z,\delta t)=\exp[-\delta t V_{\text{ab}}(z)] \quad \text{for } z_{\text{ex}}<|z|<z_{\text{in}}, \tag{8}$$

$$f(z,\delta t)=1 \quad \text{for } |z|<z_{\text{ex}}, \tag{9}$$

and

$$f(z,\delta t)=0 \quad \text{for } |z|>z_{\text{in}}. \tag{10}$$

Our calculation scheme relies on the assumption that in the asymptotic zone (defined by $|z|>z_{\text{ex}}$) the Coulomb potential can be neglected. However, the laser field may still be on. This allows us to perform the time evolution exactly even in presence of a laser pulse over arbitrary time intervals by calculating first the wave function in the velocity gauge $\psi_v(z,t)$ with the help of the formula

$$\psi_v(z,t)=\exp[-i\Delta(t,0)z]\psi_{\text{ex}}(z,t), \tag{11}$$

where

$$\Delta(t_2,t_1)=-\int_{t_1}^{t_2}E(t)dt=[A(t_2)-A(t_1)]/c \tag{12}$$

is the electric field area over the interval t_1,t_2 (or a difference in the electromagnetic vector potential A). Next we calculate the Fourier transform $\varphi_v(p,t)$ of $\psi_v(z,t)$, which evolves in time according to the equation

$$\varphi_v(p,t_2)=U(t_2,t_1)\varphi_v(p,t_1), \tag{13}$$

where the exact field propagator U is given by

$$U(t_2,t_1)=\exp\left(-\frac{i}{2}\int_{t_1}^{t_2}[p^2+2\Delta(t,0)p+\Delta^2(t,0)]dt\right). \tag{14}$$

Our method differs therefore from Millack's approach [14] by neglecting the Coulomb potential, a valid approximation for $r\gg\alpha_0$, and by using the Volkov state propagator (14). Thus our matching is performed during the laser pulse. In our algorithm we perform the series of following operations at each time $t_k=k\delta t$:

(i) The exact time evolution (including field plus Coulomb potential) of ψ_{in} is evaluated in the internal zone ($|z|<z_{\text{in}}$) using the split-operator spectral method, as originally applied to H_2^+ [29].

(ii) The outgoing wave is eliminated gradually from the internal zone with the help of Eq. (6).

(iii) The function splitting operation described by Eq. (7) is performed to provide the outgoing wave ψ_{ex} defined in the ''matching zone,'' $z_{\text{ex}}<|z|<z_{\text{in}}$.

(iv) The velocity gauge wave function ψ_v (in the external region) and its Fourier transform φ_v are calculated in the overlap region

$$\varphi_v(p,t_k)=(2\pi)^{-1/2}\int_{z_{\text{ex}}}^{z_{\text{in}}}\exp(-ipz)\psi_v(z,t_k)dz. \tag{15}$$

(v) The momentum wave function $\varphi(p,t_f)$ is propagated to some final time $t_f\geqslant t_p$ (at which the photoelectron spectra are to be calculated), using the exact formula

$$\varphi_v(p,t_f)=U(t_f,t_k)\varphi_v(p,t_k). \tag{16}$$

(vi) The momentum wave function $\varphi_v(p,t_f)$ is added to $\varphi_v^{(k-1)}(p,t_f)$'s accumulated at previous steps, i.e.,

$$\varphi_v^{(k)}(p,t_f)=\varphi_v^{(k-1)}(p,t_f)+\varphi_v(p,t_f).$$

(vii) The loop ends here and calculation starts at step (i) with the integer k replaced by $k+1$.

The most difficult part of the scheme presented here is the choice of the free parameters: V_{abs}, δt, z_{in}, and z_0. Several obvious necessary (but not sufficient) physical conditions should be satisfied. First, the external zone ($|z|>z_{\text{ex}}$) in our scheme is the asymptotic region in which we neglect the

TABLE I. Values of parameters (in atomic units) used in the wave-function splitting scheme. $n_{\rm in}$ is the number of electronic grid points in the internal zone ($|z|<z_{\rm in}$), and $n_{\rm ex}$ external grid points in momentum space with the momentum resolution $\Delta p=2\pi/7168$ a.u. n_R is the proton grid points.

dt	δt	dz	$z_{\rm ex}$	z_0	$n_{\rm in}$	$n_{\rm ex}$	$V_{\rm abs}$	$R_{\rm max}$	n_R
0.03	4.5	0.25	512	150	4196	7168	2	70	840

Coulomb forces; therefore, we must require that at $z=z_{\rm ex}$ the Coulomb force is much less then the electric force eE_M, i.e.,

$$\frac{e^2}{z_{\rm ex}^2}\leqslant eE_M. \tag{17}$$

Second, our scheme is based on the assumption that the wave entering the ''matching'' zone (of length z_0) does not return back to the nucleus, as well as that the wave exiting this zone does not return to it. This means that we should require that the classical ponderomotive radius α_0 is much smaller than the location of the beginning of the external box $z_{\rm ex}$ and also smaller than the size of the matching ''zone'' z_0:

$$\alpha_0\leqslant z_{\rm ex} \quad \text{and} \quad \alpha_0\leqslant z_0, \quad \text{where } \alpha_0=\frac{eE}{m\omega^2}. \tag{18}$$

Conditions (17) and (18) also ensure that all possible interferences in the continuum (which are expected to take place in the near-nuclei zone) are appropriately taken into account by the exact algorithm used in the internal zone. In addition, we must require that the matching should be redone after the time interval δt shorter than the time necessary to move for the fastest electron across the matching ''zone.'' Assuming that the fastest electron has the energy $E_{\rm max}=8U_p$, we thus obtain

$$\delta t\leqslant\frac{z_0}{4\sqrt{mU_p}}. \tag{19}$$

In our calculations, δt is also much less than the laser cycle. Finally, the absorption should occur on the distance z_0 longer that de Broglie wavelength of the slowest electron. Assuming that the slowest electron has the energy $\hbar\omega$, we thus obtain

$$z_0\geqslant\pi\left(\frac{2}{(\hbar\omega)}\right)^{1/2}. \tag{20}$$

For the maximal laser intensity chosen in this paper, $I=2.0\times10^{14}$ W/cm^2 and the wavelength $\lambda=600$ nm, the values of two relevant parameters are $\alpha_0=13.1$ a.u., $U_p=0.24$ a.u. $=6.5$ eV, and $\omega=0.076$ a.u.$=2.066$ eV. In Table I we list the values of all parameters which we used in our calculations and which satisfy all inequalities Eqs. (17)–(20).

The spectra of ionized electrons, defined for each R (i.e., the simulation was performed for each fixed R separately), were calculated according to the formula

$$S(E,R)=(|\varphi_{v+}(p(E),t_f)|^2+|\varphi_{v-}(p(E),t_f)|^2)\,\frac{m}{p(E)}, \tag{21}$$

where φ_+ (φ_-) are wave functions corresponding to the electron moving in the direction of positive (negative) direction along the z axis, respectively, and $p(E)=\sqrt{2mE}$. We have checked the method by comparing our results for a 1D H atom with those of Refs. [23,14] and with the results from the one-box calculations. Slight disagreement between the heights (not positions) of several first photoelectron peaks was seen if our spectra were calculated right at the end of the pulse. This disagreement disappears when the spectra are calculated at later times, $t_f>t_p$ (with the laser turned off for $t_f>t_p$), since then all slow electrons have enough time to leave the matching zone. Therefore, in all calculations we allow the system to evolve without the laser field for several subsequent cycles, and then calculate the ATI spectra (see Ref. [10] for more details).

This new two-box integration technique was first applied for calculating the ATI spectra from a H_2^+ molecule frozen at an internuclear distance R [10], and those results were used later for comparison with the full non-Born-Oppenheimer calculations, presented in the next sections.

III. A NON-BORN-OPPENHEIMER 1D MODEL OF H_2^+ IN INTENSE LASER FIELDS

We have numerically solved the complete, three-body, time-dependent Schrödinger equation for moving electrons and nuclei (in a.u.):

$$i\,\frac{\partial\psi(z,R,t)}{\partial t}=H(z,R,t)\,\psi(z,R,t), \tag{22}$$

where

$$H(z,R,t)=H_R(R)+V_C(z,R)+H_z(z), \tag{23}$$

$$H_z(z)=-\beta\,\frac{\partial^2}{\partial z^2}-\kappa zE(t), \quad H(R)=-\frac{1}{m_p}\,\frac{\partial^2}{\partial R^2}+\frac{1}{R}, \tag{24}$$

$$\beta=\frac{(2m_p+m_e)}{4m_pm_e}, \quad \kappa=1+\frac{m_e}{2m_p+m_e} \tag{25}$$

and m_e and m_p ($m_e=1$ in a.u.) are, respectively, the electron and proton masses. Hamiltonian (23) is the *exact* three-body Hamiltonian obtained after separation of the center-of-mass motion [6]. The time evolution of the internal wave function $\psi_{\rm in}$ was performed in the same way as described in Refs. [29, 6] (using the split-operator method), whereas the external part (recovered from the absorber at each δt step) $\varphi^{(k)}(p,R,t)$ was evolved with the help of the propagator, Eq. (14), for times t_1 and $t_2=t_1+\delta t$, where $\delta t=150dt$ (as previously). After each ''large'' time step δt was accomplished the new portion $\varphi(p,R,t+\delta t)$ was added to the previously

accumulated portion. The operation $\exp[-idtH(R)]$ was applied to the accumulated part of $\varphi^{(k)}(p,R,t)$ at each ''small'' time step dt, thus preserving the nuclear part. The potential $V_C(z,R)$ was neglected in the external zone, whereas the Coloumb repulsion $1/R$ was retained in $H(R)$.

We have used laser pulses of total duration 20 cycles (40 fs), having the wavelength $\lambda = 600$ nm, with a five-cycle rise and fall. The values of various parameters used in the present calculations are given in Table I. We numerically performed the time evolution of the wave functions $\psi_{\text{in}}(z,R,t)$ and the external $\varphi(p,R,t)$ for an additional two cycles (6 fs), i.e., up to the final time $t_f = 23$ cycles, using the Hamiltonian without the electric field, in order to allow some more electron-proton wave to leave the interaction region.

The initial wave function at $t=0$ was assumed to be in the following form:

$$\psi(z,R,0) = \chi(R)\psi_0(R,z) \tag{26}$$

where $\psi_0(R,z)$ was the eigenfunction of the electron Hamiltonian in H_2^+ (without the laser field) at fixed R. Two distinct initial conditions, at $t=0$ were used.

(i) H_2^+ was initially prepared in its vibrational $v=6$ $\chi(R)=\chi_6(R)$ state, which is in resonance with the 600-nm excitation,

(ii) At $t=0$, H_2^+ was prepared in a superposition of H_2^+ vibrational states, obtained by Franck-Condon excitation from the ground vibrational, $v=0$, state of the H_2 molecule, i.e.,

$$\chi(R) = \chi_0^{H_2} = \sum_{v=0} c_v \chi_v(R), \tag{27}$$

where

$$c_v = \int_0^\infty dR\ \chi_v(R)\chi_0^{H_2}(R) \tag{28}$$

are the Franck-Condon factors displayed in Fig. 2. The latter initial condition, (ii) is close to the experimental situation, in which H_2^+ is prepared by a steeply rising edge of a pulse, which rapidly ionizes the H_2 molecule.

In order to interpret the full calculation results, we first calculated the ionization rates for 170 values of R, frozen in the range from 3 to 33 a.u. The ionization rates for the laser wavelength $\lambda = 600$ nm are displayed in Fig. 3 and compare well to previous 3D calculations [7]. One observes strong CREI peaks around 7 a.u., which were discussed recently [15–19] in relation to harmonic generation and Coulomb explosion. The CREI effect manifests itself as a strong peak for the relatively low intensity $I \geqslant 5\times10^{13}$ W/cm^2, whereas at $I=4\times10^{14}$ W/cm^2 the ionization rate increases rapidly around $R=4$ a.u. and reaches a plateau with a rate close to the H-atom rate with no sharp peaks. Note that, in addition to those peaks some unexpected features appear for larger R values, in particular for lower intensities, $I=5\times10^{13}$ W/cm^2 one observes a deep minimum in the ionization rate at $R=16$ a.u. This originates from the fact that an ionizing electron from one proton comes under the influence of the second proton, and does not have enough time to escape from the second proton, before the electric field

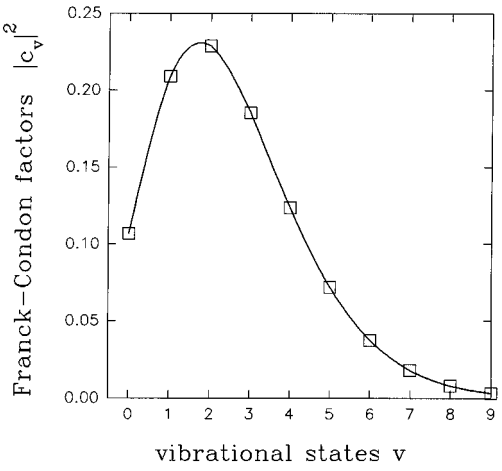

FIG. 2. Populations of initial vibrational states $|c_v|^2$ used in calculations presented in Figs. 4(b) and 5(b). The coefficients c_v are Franck-Condon factors given by Eq. (27), obtained by projecting the ground-state vibrational wave function of H_2 on the vibrational states v of H_2^+.

changes sign. Thus this electron becomes ''trapped'' between the two protons. One may expect that the position of this minimum is proportional to the classical radius of the electron in the laser field α_0.

This is indeed confirmed by the position of this minimum for an intensity twice as high, which occurs $\sqrt{2}$ times further. We are currently attempting to explain this minimum using classical dynamics of the electron.

Having calculated the wave function for each time t, we calculated the following two joint probabilities as functions of time (by integrating $|\psi|^2$ over specific regions in space), which are measures of the ionization probability $P_I(t)$ and the probability of survival defined in the following way (see Ref. [7] for more details): $P_I(t) = \text{Prob}(|z|>362$ integrated over all R's and $P_S(t) = \text{Prob}(|z|<32$ a.u., $R<10$ a.u., i.e., $P_S(t)$ is the probability of finding the electron and protons

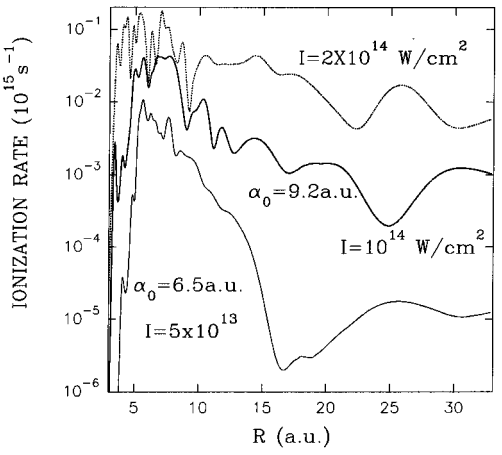

FIG. 3. Ionization rates as a function of internuclear distance for laser intensities: $I=5\times10^{13}$, 10^{14}, and 2×10^{14} W/cm^2, and $\lambda = 600$ nm. $\alpha_0 = eE/m\omega^2$ is the ponderomotive (quiver) amplitude.

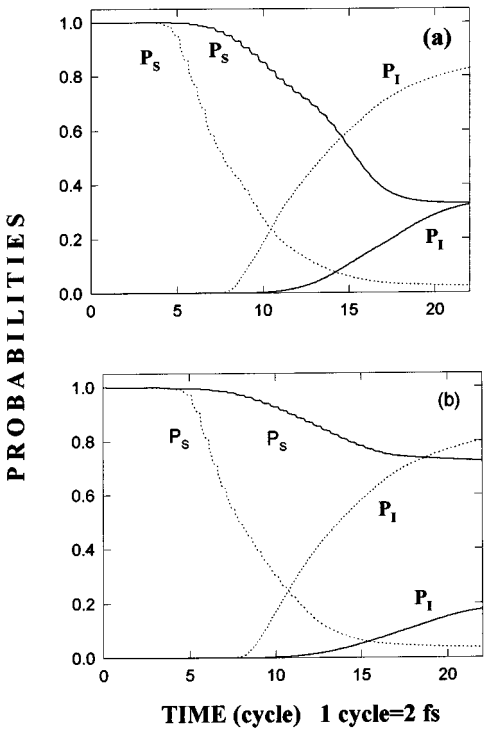

FIG. 4. Time dependence of the ionization probability $P_I(t)$ and of the probability of survival of H_2^+ $P_S(t)$. The numerical simulation was initialized either (a) from the $v=6$ state of the H_2^+ or (b) from the Franck-Condon superposition of vibrational states of H_2^+, defined by Eqs. (26) and (27). Laser intensities used: (_____) $I=10^{14}$ W/cm^2, and (.....) $I=2\times10^{14}$ W/cm^2; $\lambda=600$ nm.

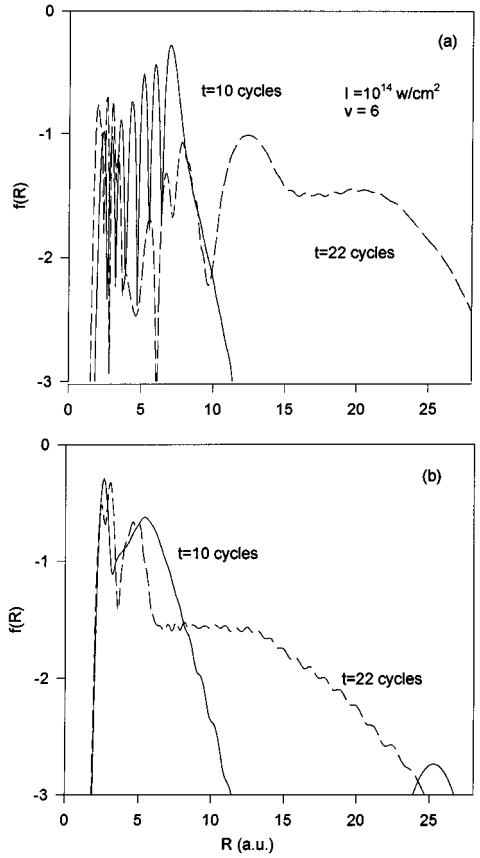

FIG. 5. Probability density $f(R)$ of finding protons at distance R for the laser intensity $I=10^{14}$ W/cm^2, $\lambda=600$ nm, calculated at $t=10$ and 22 cycles. The numerical simulation was initialized either (a) from the $v=6$ state of the H_2^+ or (b) from the Franck-Condon superposition of vibrational states of H_2^+, defined by Eqs. (26) and (27)

close to the protons center of mass. Both these numbers are measures of two possible channels: $p+p+e$, H_2^+ respectively, and consequently $1-P_S-P_I$ is a measure of the $p+H$ channel. $P_I(t)$ and P_S are plotted in Fig. 4 for all conditions considered in this paper. We observe that already at the laser intensity $I=10^{14}$ W/cm^2 the survival probability by the end of the pulse is very small (note that the amplitude of our pulse starts to decrease at $t=15$ cycles and is zero at $t=20$ cycles), and one may expect that it would be zero if the pulse would not be turned-off. Both dissociation channels, $p+H$ and $p+p+e$, have almost equal branching ratios for $I=10^{14}$ W/cm^2. The situation changes dramatically for higher intensities (see dotted lines in Fig. 4), when the H_2^+ molecule does not survive the laser field and the ionization channel $e+p+p$ dominates.

In order to have some information about the expansion of the nuclear wave function, we have integrated $|\psi|^2$ over the electron variable (i.e., over z in the internal box and over p in the external box) and thus obtained the probability density $f(R)$ of finding the nuclear fragments separated by a distance R. We have calculated $f(R)$ at $t=10$ and 22 cycles (note that the pulse was completely turned-off at $t=20$ cycles). Figures 5 and 6 show $f(R)$ functions for laser intensities $I=10^{14}$ and 2×10^{14} W/cm^2 respectively. We observe a considerable sensibility of the wave-packet evolution on the initialization of the calculation at lower intensity $I=10^{14}$ W/cm^2: there is much more dissociation, and the nuclear wave packet is much more advanced in the case $v=6$ initialization than for the Franck-Condon initialization. However, for higher intensity the shape of the $f(R)$ function depend little on the initialization. In this latter case, the nuclear has moved very far forward at time $t=22$ cycles$=44$ fs, up to 40 a.u. Also, the outgoing part of the wave packet is already well separated from a part containing surviving bound states of the H_2^+ molecule.

IV. KINETIC-ENERGY SPECTRA OF DISSOCIATING NUCLEAR FRAGMENTS

The wave functions $\psi_{\text{in}}(z,R,t_f)$ and $\varphi(p,R,t_f)$ allow us to calculate separately spectra of nuclear fragments, $S_{\text{in}}(p_R,t_f)$ and $S_{\text{ex}}(p_R,t_f)$, originating from internal and external boxes, where p_R is the relative momentum of dissociating fragments, by simply calculating the Fourier transform (with respect to the nuclear degrees of freedom) of the asymptotic part (large R) of $\psi_{\text{in}}(z,R,t_f),\varphi(p,R,t_f)$, and next calculating the square of absolute values of Fourier transforms, and integrating over electronic degrees of freedom. Formula (9) of our previous paper, Ref. [7], gives the details of calculation of the outgoing part of the wave function (this was done by cutting smoothly the wave functions in the region of small R, $R<9.5$ a.u., in order to eliminate from the proton spectrum the vibrational bound states of H_2^+).

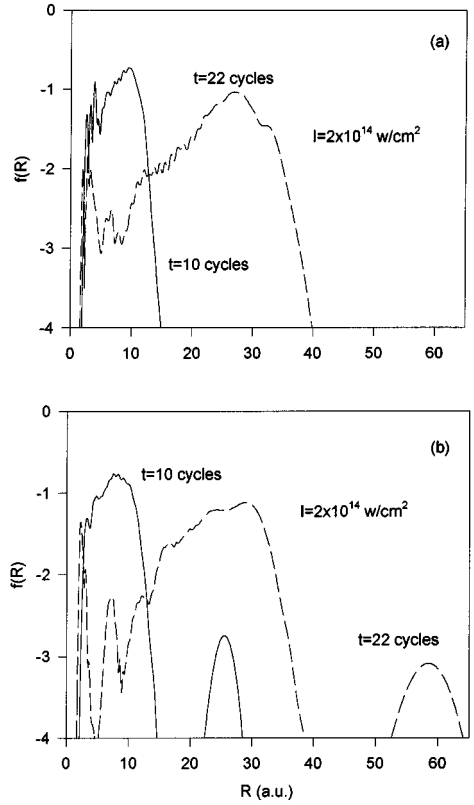

FIG. 6. Same as in Fig. 5, but for the laser intensity $I=2\times10^{14}$ W/cm^2; $\lambda=600$ nm.

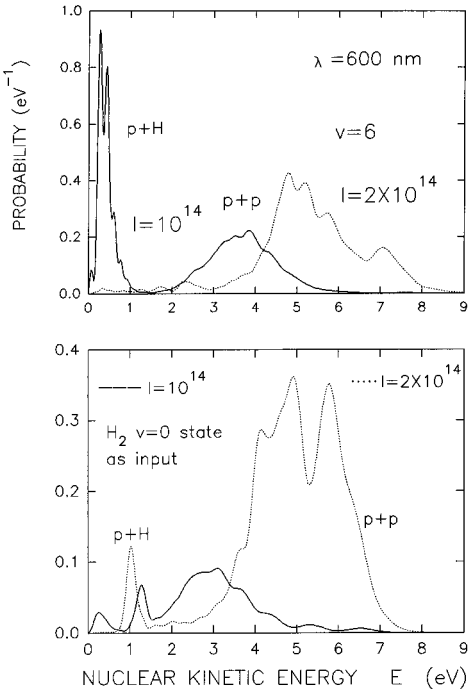

FIG. 7. Kinetic-energy spectra of dissociating nuclear fragments. The numerical simulation was initialized either (a) from the $v=6$ state of the H_2^+ or (b) from the Franck-Condon superposition of vibrational states of H_2^+, defined by Eqs. (26) and (27). Laser intensities used: (____) $I=10^{14}$ W/cm^2, and (.....) $I=2\times10^{14}$ W/cm^2; $\lambda=600$ nm.

$S_{\rm in}(p_R,t_f)$ means the joint probability of finding fragments with the relative momentum p_R and the electron within the interval $|z|<z_{\rm ex}=362$ a.u., whereas $S_{\rm ex}(p_R,t_f)$ means the joint probability of finding fragments with the relative momentum p_R and the electron outside the above interval, i.e., at $|z|>z_{\rm ex}=362$ a.u.. Thus $S_{\rm ex}(p_R,t_f)$ is a measure of the Coulomb explosion channel since it gives the probability of finding the electron far from both protons (the protons in our simulation never move further than 80 a.u.), and $S_{\rm in}(p_R,t_f)$ is a measure of dissociation channel $p+H$, since at sufficiently large t_f the ionizing electron had enough time to escape the internal box, The total spectra (i.e., containing both channels)

$$S(E)=[S_{\rm in}(p_R(E),t_f)+S_{\rm ex}(p_R(E),t_f)]\mu/p_R(E), \quad (29)$$

where $E=p_R^2/2\mu$ is the fragments relative kinetic energy (i.e., the sum of kinetic energies of both fragments in their center-of-mass system), are plotted in Fig. 7.

Two different initial conditions were used in our calculations (see Sec. III for a description of these conditions), on which the spectra depend strongly. In Fig. 7(a) we show spectra obtained from H_2^+, which initially, at $t=0$, was prepared in its vibrational $v=6$ state (two laser intensities were used $I=10^{14}$ and 2×10^{14} W/cm^2) whereas in Fig. 7(b) we show the spectra resulting from H_2^+ prepared, at $t=0$, in a superposition of vibrational states, coinciding with the ground vibrational state of the H_2 molecule, multiplied by the electronic wave function of H_2^+; see Eqs. (26)–(28). Figures 8 and 9 show the same total spectra but on a logarithmic scale (solid lines). The dotted lines in these last two figures are $S_{\rm in}$ functions, which according to the discussion in the begining of this section are measures of the $H+p$ channels. Since dotted and solid lines coincide for $E<1.5$, we conclude that the lower part of the spectrum is dominated by the $H+p$ channel or ATD, whereas the peaks for $E>2$ eV are predominantly $p+p+e$ channel peaks, i.e., Coulomb explosion. The low-energy peaks, seen in Fig. 7 are related to the bond-softening mechanism [4,27]: in Fig. 7(a) there are two very close peaks at 0.26 and 0.43 eV. Their position is close to the net absorption of one photon via a multiphoton tunnelling [7] process from the $v=6$ state. The energy released into the dissociation channel from this process, when initially the molecule was in its vibrational state v, is given by a simple, conservation energy formula

$$E=n\hbar\omega-D_v, \quad (30)$$

where $D_v=-I_p-E_v$ is the dissociation energy from the vibrational level v, $I_p=0.67$ a.u. is the ionization potential of 1D H atom, E_v is the energy of the vibrational level v of H_2^+ (from which photons are absorbed), and n is the net number of absorbed photons (in general, it is a multiphoton process: an absorption of m photons followed by the reemision of k photons, with the condition that $n=m-k>0$).

The values of dissociation energies in our 1D model are given in Table II. In general, they exceed the experimental values by 0.23 eV. For the wavelength $\lambda=600$ nm used in the present work, $\hbar\omega=2.066$ eV. Thus from $v=6$, for $n=1$, a peak at 0.542 eV is expected, and from $v=5$, a peak at

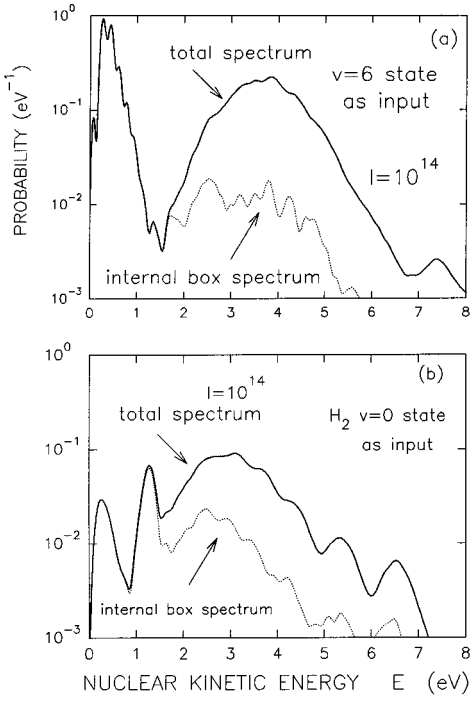

FIG. 8. Kinetic-energy spectra of dissociating nuclear fragments. The numerical simulation was initialized either (a) from the $v=6$ state of the H_2^+ or (b) from the Franck-Condon superposition of vibrational states of H_2^+, defined by Eqs. (26) and (27). Laser intensity $I=10^{14}$ W/cm^2, $\lambda=600$ nm. (.....): $H+p$ channel spectrum described by $S_{\rm in}[p_R(E),t_f i]$, (____): total spectrum (both channels).

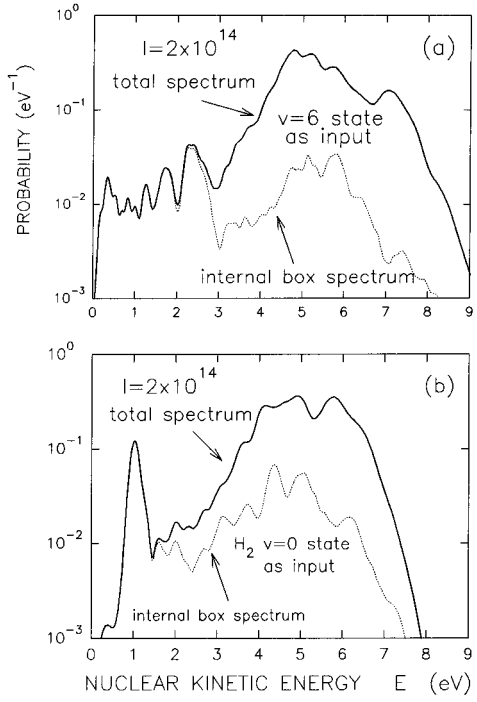

FIG. 9. Same as in Fig. 8, but for the laser intensity $I=2\times10^{14}$ W/cm^2; $\lambda=600$ nm.

0.343 eV. Two factors may be responsible for the fact that in our simulation two peaks are seen, instead of one expected at 0.542 eV: (i) first, a rapid rise, in five cycles, can populate the neighboring $v=5$ state (or, in other words the peak is shifted by the fact that our pulse is spectrally very broad); and (ii) the downward Stark shift of the level $v=6$ occurs. Further weak side peaks are also visible and correspond to excitation of other neighboring v levels. Similarly, the second low-energy peak seen in Fig. 7(b) originates from a net two-photon ATD absorption from low vibrational states: using $n=2$, and $v=0$, 1, or 2, one obtains the peak positions at 1.25, 1.50, or 1.74 eV, respectively, whereas the simulation (which used the H_2 $v=0$ state, as initial input for the vibrational wave function) yields a broad peak at $E=1.06$ eV. Again, a considerable spectral width of our pulse and the Stark shifts are the main reason of the observed discrepancy between the position of expected and seen peaks, i.e., the presence of photons having frequency only 5% less than the carrier frequency can shift the peak by 0.2 eV or more, and thus explain the observed shifts. These low-energy ATD peaks are thus consistent with a laser-induced avoided-crossing mechanism between the $1\sigma_g$ and $1\sigma_u$ potential surfaces (see Fig. 3 [7]).

TABLE II. Dissociation energies D_v (in eV) from vibrational levels v_a.

v	0	1	2	3	4	5	6	7
D_v	2.88	2.63	2.39	2.16	1.94	1.73	1.52	1.33

The high-energy broad peaks, $E>3.8$ eV, represent the $p+p+e^-$ Coulomb explosion channel, since in our calculation they originate from the external part of the wave function $\varphi(p,R,t_f)$ (see Figs. 8 and 9), in which the solid lines are much higher than dotted lines (the latter representing the $H+p$ channel). At laser intensity $I=10^{14}$ W/cm^2 we see a broad peak at $E=3.8$ eV. If the Coulomb explosion ocurred with an initial kinetic energy equal to zero, then we can conclude that the Coulomb explosion should be initiated at $R=R_c=7.16$ a.u., in order to release the Coulomb energy $E_{\rm Coulomb}=3.8$ eV (according to the relation $E_{\rm Coulomb}=27.21\ {\rm eV}/R_c$, where R_c is in a.u.), which is in agreement with Fig. 3, in which three peaks are seen at 5.6, 6.8, and 7.6 a.u. If, in addition, one takes into account the fact that at $R=R_c$ the dissociating $H+p$ have an initial nonzero kinetic energy [varying between 0.2 and 0.8 eV; see the first peak in Fig. 7(a)], one can easily understand the appearance of a broad peak centered at 3.8 eV: the explosions from the three CREI peaks seen in Fig. 1 will merge into one broad structure.

At higher intensities, Fig. 3 shows a considerable shift of CREI peaks toward lower values of R, in agreement with the shift of the Coulomb explosion peak resulting from our calculations, seen in Fig. 7, which is now centered at $E=4.8$ eV and is broader than at the lower intensity. It extends up to 8 eV, which agrees well with the lower limit of the CREI peak in Fig. 3, which is sharply cut at 3.5 a.u. Summarizing, the broad peaks in the $p+p$ channel seen in Fig. 3 agree well with the expectations for the CREI peaks based on the model with frozen nuclei [15–17]. We conclude that the position of this broad peak moves to higher energies

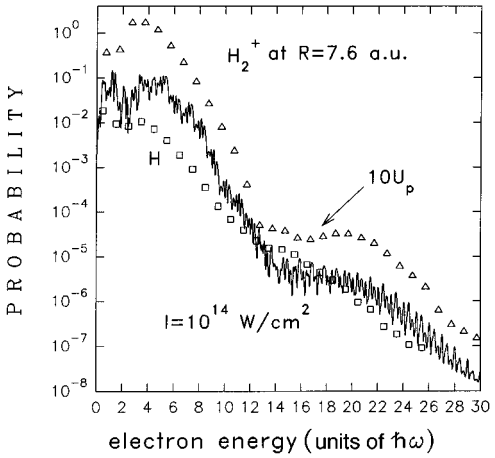

FIG. 10. ATI photoelectron kinetic-energy spectrum (in units of photon energy) from H_2^+ complete non-Born-Oppenheimer calculations (____), compared with spectra of the nuclei frozen at $R=R_c=7.6$ a.u. (△△△) and with spectra of a 1D H atom (□□□), at laser intensity $I=10^{14}$ W/cm^2; $\lambda=600$ nm. The simulation was initialized from the $v=6$ state of H_2^+. All spectra are normalized: the area under each curve is equal to the ionization probability P_I.

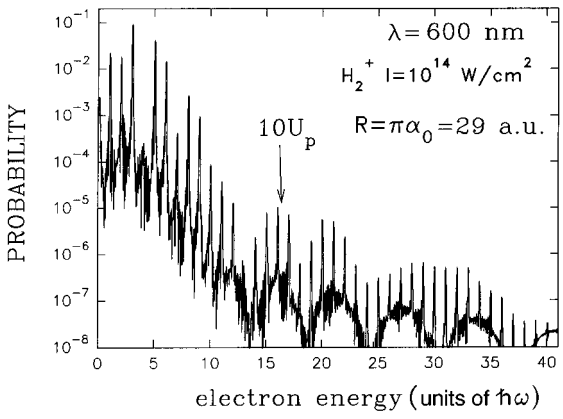

FIG. 11. ATI photoelectron kinetic-energy spectrum (in units of photon energy) from H_2^+ frozen at $R=\pi\alpha_0$ for $I=10^{14}$ W/cm^2; $\lambda=600$ nm.

when one increases the laser intensity, in accordance with recent experimental results (for a $\lambda=800$ nm laser) reported in Ref. [30]. This corresponds to smaller R_c values (Fig. 2). We would like to emphasize how useful the wave function splitting technique is for calculating proton spectra in the $p+p$ channel. This is clearly seen in Figs. 8 and 9 by comparing dotted lines with solid lines. In fact the dotted lines represent a calculation with the absorbing boundaries (with the absorption occuring in the interval $362\text{ a.u.}<|z|<512$ a.u.), whereas the solid lines describe the total spectra calculated using the wave-function splitting technique. The total spectrum is, in the high-energy part, over one order of magnitude higher than the spectrum obtained from the internal box (i.e., using absorbing boundaries).

V. ELECTRON KINETIC-ENERGY SPECTRA

The ATI spectra presented in this section were obtained by integrating over the nuclear distance R the formula (21), in which the external box function $\varphi(p,R,t_f)$, obtained from the complete, non-Born-Oppenheimer calculation was used. The normalized (i.e., the area under the spectrum curve is the ionization probability P_1) ATI spectra are shown in Fig. 10 ($I=10^{14}$ W/cm^2). Our exact non-Born-Oppenheimer results (solid lines) are compared with the ATI spectra originating from the 1D H atom (□□□) and from H_2^+ frozen at $R=R_c$ (△△△). One notes a considerable enhancement of the spectrum around $3U_p$, and enhancement at very large energies, up to $16U_p$ for the lower laser intensity. A frozen nuclei calculation also shows such enhancement at particular large distances (33 a.u. or more [11]), which are close to integer multiples of the classical ponderomotive radius α_0. Classical trajectory calculations show that an electron reaches its maximal kinetic energy at distances $z_{\max}$ given in Refs. [31, 32],

$$z_{\max}=(2n+1)\pi(v_0/\omega+\alpha_0), \tag{31}$$

where v_0 is the electron's initial velocity. We have calculated the ATI spectra generated by H_2^+ frozen at various R's, and verified that indeed a very long tail appears in the ATI spectra, extending much farther than the spectrum from the H atom, for R values exceeding α_0. We display in Fig. 11 the ATI spectrum generated by H_2^+ frozen at $R=\pi\alpha_0=29$ a.u., since at this distance a particularly long tail in the spectrum is expected from formula (31). Indeed, a clear pla-

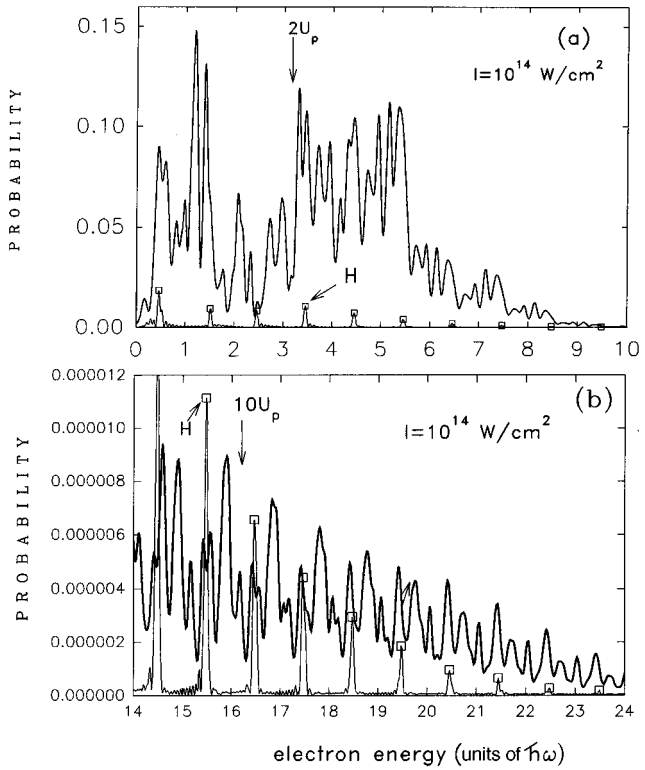

FIG. 12. (a) The low-energy part of ATI spectra from Fig. 10. (b) The high-energy part of ATI spectra from Fig. 10.

teau appears in the spectrum extending up to $15U_p$. Comparing Figs. 10 and 11 indicates that most of the ATI is due to CREI at $R_c=7$ a.u. Also in Fig. 12, we display the low- ($<3U_p$) and high-energy ($>10U_p$) parts of the ATI spectrum in order to emphasize the details of the spectrum. One observes that there are more peaks in the molecular spectrum than in the atomic (or in the frozen molecule) ATI spectra.

VI. CONCLUDING REMARKS

We have shown in the present work that dissociative ionization of the molecular ions contains much new information about electron-nuclear dynamics. Thus from our full non-Born-Oppenheimer TDSE of H_2^+ we have been able to calculate ATD, Coulomb explosion, and accompanying ATI probabilities. The calculated-low energy ATI proton spectra agree with a dressed-state interpretation of laser-induced avoided crossings between two essential electronic potentials at high intensities. The high-energy proton spectra agree with theoretical predictions from Coulomb explosions of protons at the CREI critical internuclear distance R_c. ATI electron kinetic-energy spectra show high-energy parts up to $15U_p$ related to inelastic collisions of ionizing electrons with Coulomb exploding protons at large distances. The present wave-splitting technique, which removes absorbing boundaries and uses asymptotic matching, enables us to calculate the complete proton and electron kinetic-energy spectra, and thus constitutes a complete non-Born-Oppenheimer treatment of molecular dissociative ionization in an intense laser field.

We find that in general the non-Born-Oppenheimer ATI peaks are split in two, and are accompanied by additional peaks which cannot be correlated with vibrational structure. In the low-energy region, less than $3U_p$ (Fig. 3), one expects the electron to recollide with the molecule after half a cycle, whereas, in the $10U_p$ region (Fig. 4), the electron accelerates outwards during half a cycle [32]. Only the $10U_p$ region seems to have regular structures. Secondary strong peaks appear between the main ATI peaks. Since the initial state is an equally split wave packet ($1\sigma_g$) separated by R, one expects interferences to occur from these two sources, as opposed to single atoms, where the initial state is a single source. We have termed such interference, laser induced electron diffraction [33].

ACKNOWLEDGMENTS

The financial support from the Natural Sciences and the Engineering Research Council of Canada is gratefully acknowledged. All calculations were performed on an IBM-SP2 at the Centre d'Application de Calcul Paralelle (CACPUS).

[1] G. Mainfray and C. Manus, Rep. Prog. Phys. **54**, 1333 (1991).
[2] J. H. Eberly, J. Javanainen, and K. Rzazewski, Phys. Rep. **204**, 331 (1991).
[3] A. L'Huillier, K. J. Schafer, and K. C. Kulander, J. Phys. B **24**, 3315 (1991).
[4] *Molecules in Laser Fields*, edited by A. D. Bandrauk (Marcel Dekker, New York, 1993).
[5] *Atoms in Intense Fields*, edited by M. Gavrila (Academic, San Diego, 1992).
[6] S. Chelkowski, T. Zuo, O Atabek, and A. D. Bandrauk, Phys. Rev. A **52**, 2977 (1995).
[7] S. Chelkowski, A. Conjusteau, T. Zuo, and A. D. Bandrauk, Phys. Rev. A **54**, 3235 (1996).
[8] K. C. Kulander, F. H. Mies, and K. J. Schafer, Phys. Rev. A **53**, 2562 (1996).
[9] A. M. Popov, O. V. Tikhonova, and E. A. Volkova, Laser Phys. **7**, 108 (1997).
[10] S. Chelkowski and A. D. Bandrauk, Int. J. Quantum Chem. **30**, 473 (1996).
[11] S. Chelkowski and A. D. Bandrauk, Laser Phys. **7**, 797 (1997).
[12] R. Heather and H. Metiu, J. Chem. Phys. **86**, 5009 (1987).
[13] A. Keller, Phys. Rev. A **52**, 1450 (1995).
[14] T. Millack, Phys. Rev. A **48**, 786 (1993).
[15] T. Zuo, S. Chelkowski, and A. D. Bandrauk, Phys. Rev. A **48**, 3837 (1993).
[16] T. Zuo and A. D. Bandrauk, Phys. Rev. A **52**, R2511 (1995).
[17] S. Chelkowski and A. D. Bandrauk, J. Phys. B **28**, L723 (1995).
[18] T. Seideman, M. Ivanov, and P. B. Corkum, Phys. Rev. Lett. **75**, 2819 (1995); E. Constant, H. Stapefeldt, and P. B. Corkum, Phys. Rev. Lett. **76**, 4140 (1996).
[19] J. H. Posthumus, L. J. Frasinski, A. J. Giles, and K. Codling, J. Phys. B **28**, L349 (1995).
[20] K. J. Schafer, B. Yang, L. F. DiMauro, and K. C. Kulander, Phys. Rev. Lett. **70**, 1599 (1993).
[21] J. Z. Kaminski, A. Jaron, and F. Ehlotzky, Phys. Rev. A **53**, 1756 (1996).
[22] G. G. Paulus, W. Becker, and H. Walther, Phys. Rev. A **95**, 2851 (1994).
[23] G. G. Paulus, W. Nicklich, Huale Xu, P. Lambropoulus, and H. Walther, Phys. Rev. Lett. **72**, 2851 (1994).
[24] Y. L. Shao, T. Ditmire, J. W. G. Tisch, E. Springate, J. P. Marangos, and M. H. R. Hutchinson, Phys. Rev. Lett. **77**, 3343 (1996).
[25] P. Dietrich, D. T. Strickland, M. Laberge, and P. Corkum, Phys. Rev. A **47**, 2305 (1993); D. Normand, L. A. Lompré, and C. Cornaggia, J. Phys. B **25**, L497 (1992); E. E. Aubanel, J. M. Gauthier, and A. D. Bandrauk, Phys. Rev. A **48**, 2145 (1993); J. Shertzer, A. Chandler, and M. Gavrila, Phys. Rev. Lett. **73**, 2039 (1994).
[26] R. Numico, A. Keller, and O. Atabek, Phys. Rev. A **52**, 1298 (1995).
[27] P. H. Bucksbaum, A. Zavriyev, H. G. Muller, and D. W. Schumacher, Phys. Rev. Lett. **64**, 1883 (1990).
[28] H. Yu, T. Zuo, and A. D. Bandrauk, Phys. Rev. A **54**, 3290 (1996).
[29] S. Chelkowski, T. Zuo, and A. D. Bandrauk, Phys. Rev. A **46**, 5342 (1992).
[30] T. D. G. Walsh, F. A. Ilkov, and S. L. Chin, J. Phys. B **30**, 2167 (1997).
[31] P. Moreno, L. Plaja, and L. Roso, J. Opt. Soc. Am. B **13**, 430 (1996).
[32] A. D. Bandrauk, S. Chelkowski, H. Yu, and E. Constant, Phys. Rev. A **56**, R2537 (1997).
[33] T. Zuo, A. D. Bandrauk, and P. B. Corkum, Chem. Phys. Lett. **239**, 313 (1996).